Article

Multifunctional Sodium Gluconate Electrolyte Additive Enabling Highly Reversible Zn Anodes

ZHAO Kang[1,2], ZHAO Jianan[2], YU Meng[1], LIU Fangming[1], DONG Yang[1], WANG Shiwen[2]✉ and CHENG Fangyi[1]✉

Received April 28, 2024
Accepted May 15, 2024

Sodium gluconate (SG) is reported as an electrolyte additive for rechargeable aqueous zinc batteries. The SG addition is proposed to modulate the nucleation overpotential and plating behaviors of Zn by forming a shielding buffer layer because of the adsorption priority and large steric hindrance effect, which contributes to limited rampant Zn^{2+} diffusion and mitigated hydrogen evolution and corrosion. With the introduction of 30 mmol/L SG in 2 mol/L $ZnSO_4$ electrolyte, the Zn anode harvests a reversible cycling of 1200 h at 5 mA/cm^2 and a high average Coulombic efficiency of Zn plating/stripping (99.6%). Full cells coupling Zn anode with $V_2O_5{\cdot}1.6H_2O$ or polyaniline cathode far surpass the SG additive-free batteries in terms of cycle stability and rate capability. This work provides an inspiration for design of a high-effective and low-cost electrolyte additive towards Zn-based energy storage devices.

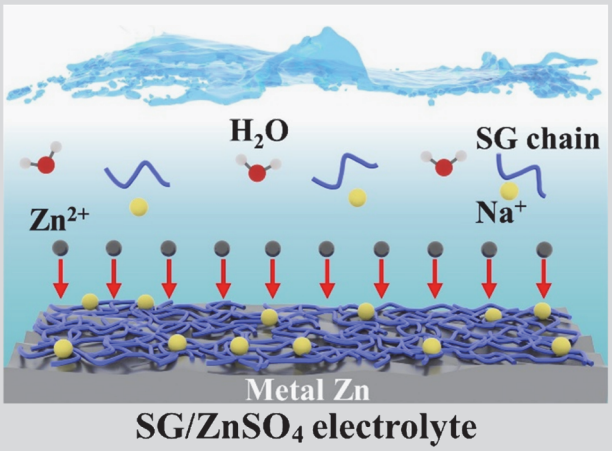

Keywords Electrolyte additive; Zn anode; Sodium gluconate; Adsorption; Zn dendrite

1 Introduction

Rechargeable aqueous zinc batteries (RAZBs) not only embrace the diverse merits of aqueous electrolyte, such as intrinsic non-flammable safety, easy operation and high ionic conductivity, but also inherit high theoretical capacity (820 mA·h/g) and low electrochemical potential (−0.76 V *vs*. standard hydrogen electrode) of metallic Zn anode.[1−3] Nonetheless, the practical applications of Zn-based batteries are significantly impeded by the persistent irreversibility of Zn metal anodes in aqueous solutions, which is attributed to rampant dendrite growth and notorious side reactions.[4−6] Specifically, hard Zn protrusions that grow perpendicularly to the anode surface could easily pierce the separator and lead to the battery failure.[7,8] Furthermore, porous Zn deposits with irregular morphologies are bound to exacerbate the H_2 generation and corrosion reactions due to the increased exposure of fresh Zn/electrolyte interfaces, which irreversibly consume electrolyte and active Zn and thus lead to performance degradation.[9,10]

Until now, valid strategies, such as 3D structural design,[11,12] interfacial modification,[13,14] and electrolyte manipulation have been implemented to overcome the drawbacks of Zn anodes.[15−17] Thereinto, electrolyte optimization only with trace additive is more appealing owing to the features of simple operation, apparent effect and cost effectiveness.[18,19] The organic electrolyte additives reported so far can be mainly divided into two categories according to different functions. One focuses on coordinating with Zn^{2+} to optimize the solvation structures, thereby alleviating the water decomposition and realizing a dendrite-free Zn anode.[20,21] The other is building a protective layer by species adsorption effect, which can tailor the anode/electrolyte interface and further improve the cycling stability of Zn deposition/dissolution.[22−24] Despite the substantial advances, most organic additives are focused on the plating process, such as Zn^{2+} desolvation, zincophilic modulation and lattice match, while the proper regulation on nucleation overpotential of metal Zn is still rare. It has been recognized that the higher overpotential would actuate the formation of smaller nucleus, which facilitates the uniform plating of Zn ions.[25] Additionally, nucleation rate increases exponentially as the overpotential increases, contributing to the generation of fine and dense Zn deposits.[26,27] Evidently, the nucleation overpotential plays a

✉ CHENG Fangyi
fycheng@nankai.edu.cn
✉ WANG Shiwen
wshwory@zzuli.edu.cn
1. College of Chemistry, Nankai University, Tianjin 300071, P. R. China;
2. College of New Energy, Zhengzhou University of Light Industry, Zhengzhou 450002, P. R. China

key role in guiding homogeneous Zn^{2+} plating, which can be adjusted to access dendrite suppressing characteristic.[28] Therefore, it is highly desirable to explore a multifunctional electrolyte additive to inhibit the dendrite formation and synchronously eliminate the water-induced parasitic reactions based on the increased nucleation overpotential.[29,30]

Herein, an easily available, low cost, environmental benign, and highly effective additive, sodium gluconate (SG), is proposed to regulate the nucleation overpotential for highly reversible Zn anodes in aqueous electrolyte. Abundant polar anions of SG could form a steric hindrance effect on the zinc anode, alleviating interfacial side reactions and increasing the overpotential of Zn plating, while free cationic Na^+ could be preferentially adsorbed on the surface of abrupt Zn protuberance and induce a dynamic electrostatic shielding layer, which hinders the agglomerative Zn nucleus. Profiting from SG additive, the Zn nucleation overpotential increases from 52.7 mV in 2 mol/L $ZnSO_4$ electrolyte to 74.2 mV after the addition of 30 mmol/L SG. Consequently, dendrite-free and uniform Zn deposits are achieved in the SG-containing electrolyte even at a large areal capacity of 20 mA·h/cm^2. The symmetric Zn/Zn cells with SG additive can withstand for 1200 h at the current density of 5 mA/cm^2, and the asymmetric Zn/Cu batteries with SG/$ZnSO_4$ electrolyte yield a considerable average Coulombic efficiency of 99.6%. Interestingly, the rationalized 2 mol/L $ZnSO_4$+30 mmol/L SG electrolyte is versatilely compatible with varied cathodes, such as V_2O_5·1.6H_2O and polyaniline. This study would provide an alternative addition for electrolyte design to enable high-performance aqueous Zn batteries.

2 Experimental

2.1 Materials and Instruments

$ZnSO_4$·7H_2O (99.995%) and sodium gluconate (SG, >99.0%) were purchased from Aladdin (Shanghai, China) and TCI Shanghai (China), respectively. Metallic foils (Zn, Ti and Cu) with high purity (99.9%) were supplied by Qingyuan Metal Materials (Xingtai, China), the thickness of Zn foil is 25 μm. Vanadium oxide (V_2O_5, 99.7%) and polyaniline (PANI, 98%) were obtained from Energy Chemical (Shanghai, China) and Macklin (Shanghai, China), respectively.

Morphological images were collected on a 3D laser confocal scanning microscope (LCSM, KEYENCE VH-Z250R) and a field-emission scanning electron microscope (SEM, JEOL JSM-7500F). The phase composition was analyzed by the X-ray diffraction (XRD, Rigaku MiniFlex 600) test using Cu *Kα* radiation. Fourier transform infrared (FTIR) spectra were collected on a spectrometer (Bruker Tensor II Sample Compartment RT-DLaTGS) in the range of 4000—400 cm^{-1}. Ionic conductivity and pH measurements were performed on a benchtop conductivity meter (REX DDSJ 308A) and a pH meter (REX PHSJ 3F) at 25 °C, respectively.

2.2 Sample Preparation

The SG/$ZnSO_4$ electrolytes at different concentrations were made from SG powder and 2 mol/L $ZnSO_4$ aqueous solution, which were formulated from certain stoichiometric ratio under ambient circumstances. The V_2O_5·1.6H_2O cathodes containing V_2O_5·1.6H_2O powders, Super-P carbon black and polyvinylidene fluoride with a mass ratio of 8:1:1 were homogeneously mixed by using *N*-methyl-2-pyrrolidone (NMP) as solvent. The electrode slurry was casted onto Ti foil (active mass loading of 1.5—2 mg/cm^2) and vacuum dried at 80 °C for 12 h. The polyaniline (PANI) electrodes were prepared by pressing the mixture of PANI, Ketjen black and polytetrafluoroethylene (PTFE) in a mass ratio of 5:4:1 on Ti mesh. The PANI loading was measured to be about 2 mg/cm^2. The V_2O_5·1.6H_2O cathode material was synthesized by a hydrothermal method. Typically, 0.36 g of V_2O_5 powder, 5 mL of H_2O_2 (30%) and 30 mL of deionized water were mixed and maintained at 190 °C for 10 h. The product was collected by vacuum filtration, washed with deionized water several times, and dried in vacuum at 80 °C for 12 h.

2.3 Electrochemical Measurements

CR2032 coin-type cells were assembled in air using a glass fiber separator. The electrochemical performances of Zn/Zn, Zn/Cu, Zn/Ti, Zn/V_2O_5·1.6H_2O and Zn/PANI batteries were tested on a LAND CT2000A. Voltammograms were collected at a scan rate of 0.5 mV/s on a Solartron 1470E electrochemical workstation. The potentiostatic current-time transient curves were recorded at a constant overpotential of −150 mV *vs*. Zn^{2+}/Zn. Electrochemical impedance spectroscopy (EIS) tests were measured at a perturbation amplitude of 5 mV ranging from 100 kHz to 0.01 Hz. The activation energy was calculated according to Arrhenius equation from EIS results.

The hydrogen evolution reaction behaviors were investigated using linear sweep voltammetry (LSV) in aqueous 1 mol/L Na_2SO_4-based solutions with a three-electrode configuration, where Ti foil, graphite rod and saturated calomel electrode (SCE) were used as working, counter, and reference electrodes, respectively. Cyclic voltammetry (CV) of Zn plating/stripping was tested in a two-electrode cell, where Ti foil served as working electrode and Zn foil as counter electrode. The phase-selective alternating current (AC) voltammetry tests were performed in asymmetric Zn/Ti cells at a scanning rate of 20 mV/s with

https://doi.org/10.1007/s40242-024-4110-9

the voltage ranging from 0.65 V to 0 V *vs*. Zn^{2+}/Zn. The frequency was 6 Hz, the amplitude (A) was 5 mV, and the selective region of phase angles was 0°—90°. The phase shift (Φ) was calculated by Equation 1:

$$\Phi = \tan^{-1}\frac{i_{90}}{i_0} \quad (1)$$

where i_0 and i_{90} are the currents at the phase angles of 0° and 90°, respectively.

The impedance (Z) was given by Equation 2:

$$Z = \frac{A}{\sqrt{i_{90}^2 + i_0^2}} \quad (2)$$

and the real (Z_{re}) and imaginary (Z_{im}) parts of the impedance were given by Equations 3 and 4:

$$Z_{re} = Z\cos\Phi \quad (3)$$

$$Z_{im} = Z\sin\Phi \quad (4)$$

The capacitance (C) can be calculated by the following Equation 5:

$$C = 1/(2\pi f Z_{im}) \quad (5)$$

where f is the frequency of the AC perturbation.

Zn^{2+} deposition barrier could be quantitatively evaluated from the temperature-dependent EIS data, according to Equation 6:

$$\ln(1/R_{ct}) = \ln A - E_a/RT \quad (6)$$

where R_{ct} is the interfacial Zn^{2+} transfer resistance, E_a is the activation energy, T is the absolute temperature, R is the gas constant, and A is the pre-exponential factor.

Coin cells (CR2032 type) of Zn/Zn, Zn/Cu, $Zn/V_2O_5{\cdot}1.6H_2O$ and Zn/PANI configurations were assembled in air atmosphere and electrochemically measured on a battery tester (LAND CT2000A). Symmetrical batteries were fabricated by sandwiching the glass fiber film (φ 16 mm) between two Zn chips (φ 12 mm) with 30 μL of electrolyte. Coulombic efficiency (CE) was evaluated on asymmetric Zn/Cu coin cells with Cu and Zn foil as the working and counter electrodes, respectively. The $Zn/V_2O_5{\cdot}1.6H_2O$ and Zn/PANI batteries were galvanostatically charged/discharged in the voltage range of 0.2—1.6 V (*vs*. Zn^{2+}/Zn) and 0.5—1.5 V (*vs*. Zn^{2+}/Zn), respectively.

3 Results and Discussion

3.1 Electrolyte Formulation

Corrosion reactions of Zn take place spontaneously once the aqueous electrolyte contacts with metallic Zn.[31,32] To evaluate the anti-corrosion effect of the SG additive, fresh Zn foils were soaked in 2 mol/L $ZnSO_4$ solutions with/without additive for 24 h. As displayed in Fig. 1A, the Zn foil immersed in $ZnSO_4$ electrolyte exhibits rough surfaces with bulk flake-like byproducts $Zn_4SO_4(OH)_6{\cdot}xH_2O$ (ZSOH). Apparently, the generation of irregular byproducts is significantly reduced after the introduction of 10 mmol/L SG

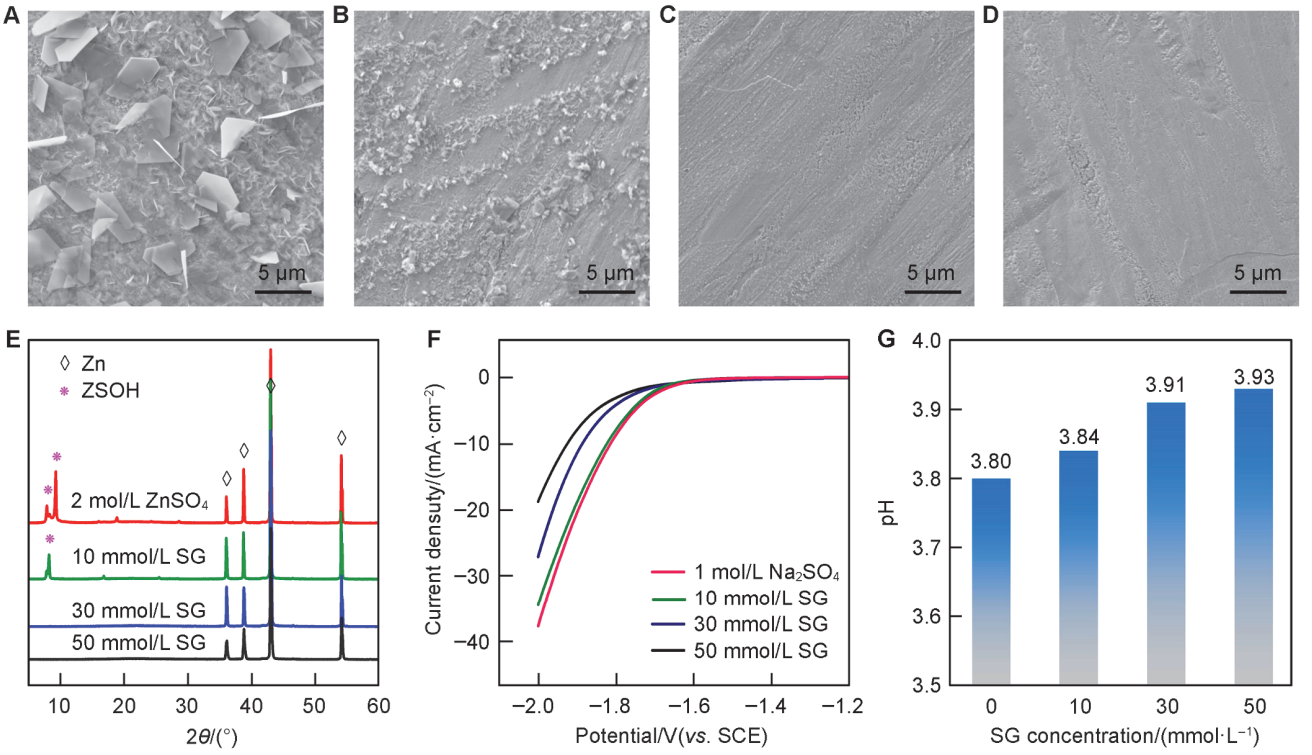

Fig. 1 SEM images of Zn foil after immersing in 2 mol/L $ZnSO_4$ (A), 2 mol/L $ZnSO_4$ with 10 mmol/L (B), 30 mmol/L (C) and 50 mmol/L (D) SG additive for 24 h, and the corresponding XRD patterns (E), linear sweep voltammetry curves recorded at 10 mV/s in SG-containing Na_2SO_4 solutions (F), and pH evolution of 2 mol/L $ZnSO_4$-based electrolytes with increased SG concentration (G)

https://doi.org/10.1007/s40242-024-4110-9

(Fig. 1B), and almost totally suppressed at the concentrations of 30 and 50 mmol/L (Fig. 1, C and D). This phenomenon can be additionally identified *via* the absence of the ZSOH peaks in XRD patterns (Fig. 1E). Furthermore, the typical FTIR signals of SG molecules instead of ZSOH species are detected on the soaked Zn anodes in 30 mmol/L additive-containing $ZnSO_4$ electrolyte, confirming the anticorrosive Zn surface achieved by the SG adsorption (Fig. S1 in the Electronic Supplementary Information, ESI).

Besides, the hydrogen evolution reaction (HER) is parasitic accompanied by Zn deposition, which elevates the local concentration of OH^- and provokes the generation of inactive byproducts.[33,34] To assess the impact of SG additive on the HER activity, linear sweep voltammetry (LSV) tests were executed in 1 mol/L Na_2SO_4-based solutions without Zn^{2+} plating. As illustrated in Fig. 1F, the hydrogen evolution potential decreases as the SG addition increases, revealing the suppression of HER behaviors. Similarly, the inhibitory effect of H_2 generation by the SG additive is versatile in $ZnSO_4$ electrolytes (Fig. S2 in the ESI). As indicated by the pH values (Fig. 1G), SG molecules would dissociate in the aqueous solutions to form free Na^+ and gluconate anions, which is beneficial to forming the molecular adsorption layer and alleviating the interfacial side reactions.[35]

The adsorption behavior of the SG molecules was further investigated by alternating current voltammetry measurements. As displayed in Fig. 2A, the capacitance values decrease gradually with the increase of SG amounts, denoting more SG molecules adsorbed on the electrode and a thicker electrical double layer, thus rendering a reduced effective electrochemical surface area at the interface.[36] The reduced capacitances could limit the reaction dynamics of rampant Zn deposition, which plays a key role in suppressing Zn dendrite formation.[37] As shown in Fig. 2B, there is insignificant difference in FTIR spectra of 50 mmol/L SG-existing solutions, further revealing that SG molecules mainly exert effect on the anode interface rather than tailoring the Zn^{2+} solvation structure. As observed in cyclic voltammetry (CV) curves, the varied peak currents reveal the different kinetics of Zn plating/stripping, which decreases with increasing SG amount (Fig. 2C). Similarly, this trend can also be detected from the voltage-time curves revealing higher nucleation overpotentials after SG addition (Fig. 2D).

From a dynamic perspective, the enhanced overpotentials could provide a sufficient driving force for the nucleation and growth with finer zinc nuclei.[38,39] Furthermore, the kinetics of Zn plating was quantitatively analyzed by the temperature-dependent EIS. Based on the charge transfer resistance (R_{ct}) of symmetrical Zn/Zn cells at diverse temperatures (Fig. S3 in the ESI), the activation energy (E_a) can be obtained by calculating the slope from

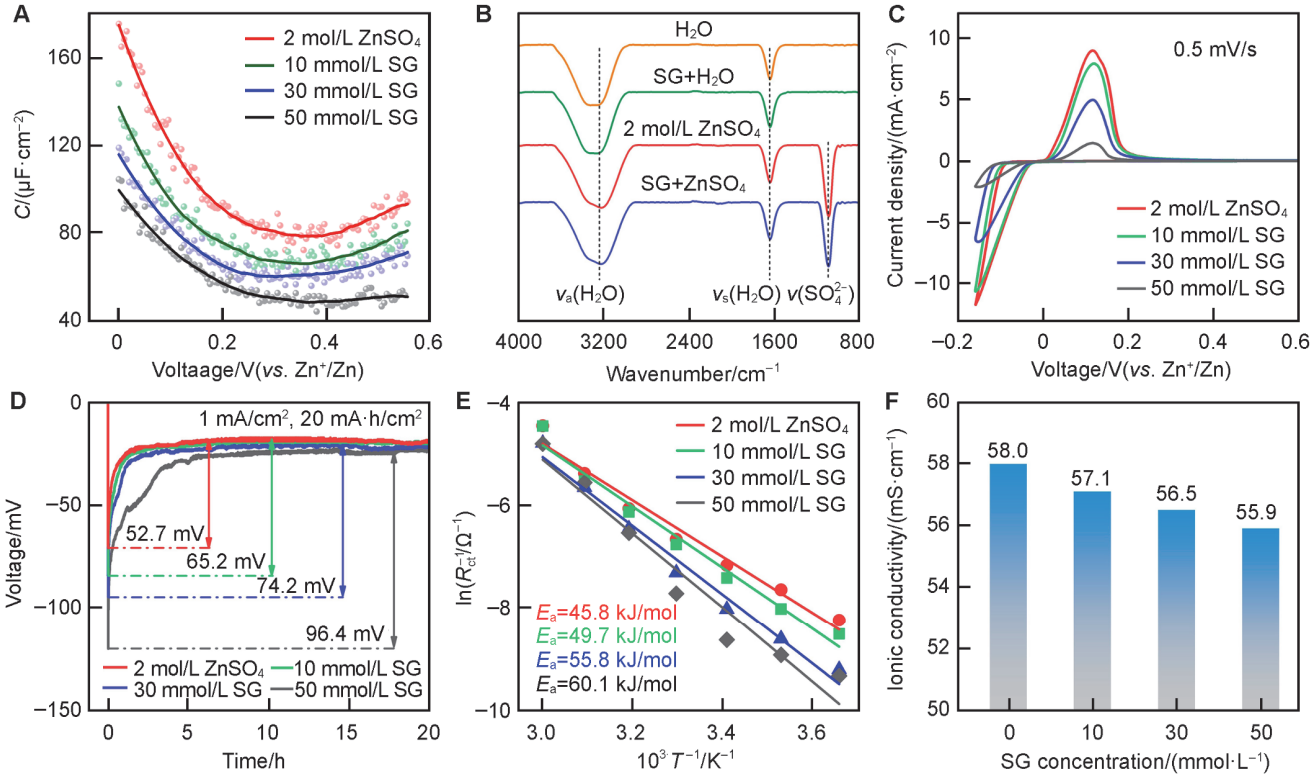

Fig. 2 Differential capacitance-potential curves of various electrolytes (A), FTIR spectra of 50 mmol/L SG-added H_2O and 2 mol/L $ZnSO_4$ solution (B), cyclic voltammograms of Zn plating/stripping (C), nucleation overpotentials based on the Cu substrate (D), Arrhenius behavior and activation energies of Zn deposition (E), and ionic conductivity tested in $ZnSO_4$ electrolytes with different amounts of SG (F)

https://doi.org/10.1007/s40242-024-4110-9

Arrhenius law (Fig. 2E). Evidently, the E_a value increases as the SG addition increases, manifesting a higher barrier of Zn deposition. Note that the ionic conductivity decreases slightly from 58.0 mS/cm to 55.9 mS/cm as a function of SG concentration (Fig. 2F). Consequently, the appropriate adsorption of SG molecules on Zn surface is expected to play a barrier role to regulate Zn plating while excessive additive will significantly reduce the reaction kinetics because of decreased ionic conductivity.[40] Taking these factors into consideration, 30 mmol/L SG additive was chosen to assess the impact on 2 mol/L $ZnSO_4$ solution.

3.2 Zn Deposition Investigations

The 3D laser confocal scanning microscopy (LCSM) was conducted to visually assess the controllable Zn deposits achieved by SG additive. As displayed in Fig. 3A, massive mossy Zn dendrites emerge on the electrode surface in pristine 2 mol/L $ZnSO_4$ electrolyte and an extremely bumpy surface can be observed at the higher plating capacity. In stark contrast, more glabrous Zn deposits are attained with the addition of 30 mmol/L SG, presenting a markedly decreased altitude intercept of 32.64 μm at 20 mA·h/cm² (Fig. 3B). The similar conclusion was also evidenced by SEM images (Fig. S4 in the ESI). Accordingly, we further recap the multiple mechanisms for stabilizing Zn anodes by SG additive. The influence of SG on the nucleation process and surface change was scrutinized by chronoamperometry (CA) at −150 mV (Fig. 3C). Clearly, a more stable current density in SG-containing electrolyte implies the stable and compact diffusion procedure with homogeneous crystal growth. Contrarily, the current density in the $ZnSO_4$ electrolyte is consistently increasing, representing a rampant diffusion behavior due to the unremitting accumulation of Zn^{2+} and further conversion to dendrites.[41]

Based on the above results, a bifunctional effect of gluconate anions and Na^+ in SG molecules emerges as the intrinsic mechanism of stabilizing Zn anodes. As shown in Fig. 3D, the heterogeneous deposition on the metal Zn surface finally leads to rampant dendrites in conventional $ZnSO_4$ electrolyte, accompanied by H_2 evolution and the byproduct formation of ZSOH. In stark contrast, the SG molecules absorbed onto Zn surface can regulate the reaction kinetics and reduce the Zn^{2+} aggregation, which will form the dense and uniform deposits (Fig. 3E). Besides, the electrochemically inert SG molecules at interfacial regions could boost the stability of Zn anodes by alleviating the parasitic reactions during Zn deposition.[42]

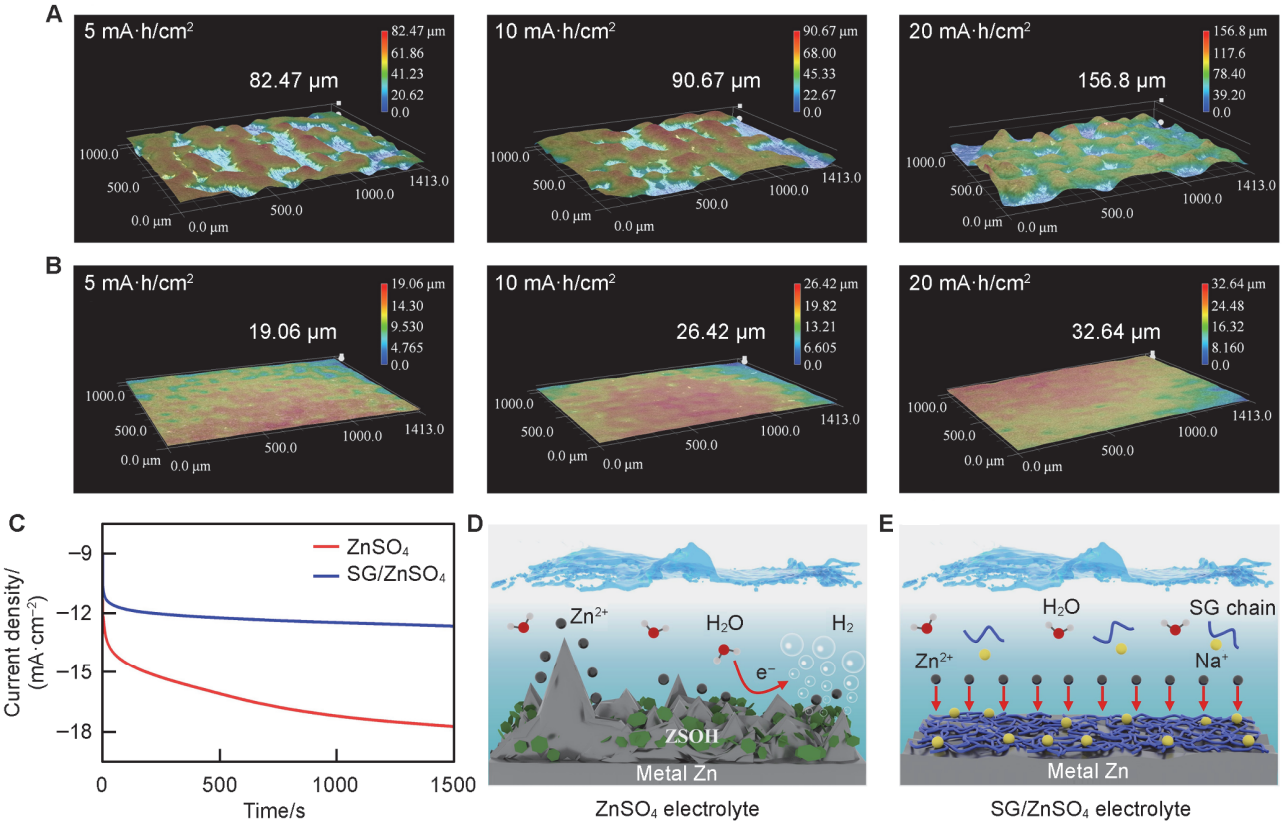

Fig. 3 LCSM surface topography of Zn deposits in $ZnSO_4$ (A) and SG/$ZnSO_4$ (B) electrolytes at 10 mA/cm² for diverse areal capacities, potentiostatic current-time transient curves of Zn deposition in $ZnSO_4$-based electrolytes with/without SG at a fixed overpotential of −150 mV (C), and schematic illustrations of Zn plating behaviors in benchmark $ZnSO_4$ electrolyte (D) and SG-functionalized $ZnSO_4$ electrolyte (E)

https://doi.org/10.1007/s40242-024-4110-9

3.3 Electrochemical Performances

The positive role of SG additive on the reversibility of Zn anodes was further verified using symmetric Zn/Zn configurations (Fig. 4A). The $ZnSO_4$ electrolyte with 30 mmol/L SG delivers a stable cycling lifespan of 300 h, much better than that with the addition of 10 and 50 mmol/L. Clearly, a small amount of SG (*e.g.*, 10 mmol/L) is insufficient to protect Zn anode, showing a poor electrochemical performance. In contrast, excessive additives (*e.g.*, 50 mmol/L) could hinder the charge transfer and Zn^{2+} diffusion, which will exacerbate the battery polarization and lead to a limited effect on the improvement of Zn anode. Not surprisingly, the Zn anode surface in neat $ZnSO_4$ electrolyte is completely covered by characteristic protrusions and flake-like ZSOH byproducts (Fig. S5 in the ESI). On the contrary, even and compact deposits on metal Zn are obtained in the presence of SG additive. More attractively, the introduction of 30 mmol/L SG additive can also support reversible plating/ stripping process at a high current density of 5 mA/cm² (Fig. 4B). Fig. 4C shows the limit current density with a fixed plating/stripping time (1 h) and a step-increased current density (0.5 mA/cm²). The SG additive significantly enhances the rate capability, showing unfluctuating charge and discharge up to 10 mA/cm². Similarly, the rate performance improved by the addition of 30 mmol/L SG is further evidenced in Fig. 4D.

Fig. 4E illustrates the reversible deposition/dissolution in asymmetric Zn/Cu cells with pristine $ZnSO_4$ electrolyte and SG/$ZnSO_4$ electrolyte. Apparently, the CE values in $ZnSO_4$ electrolyte decay quickly after 100 cycles because of dendrite growth and side reactions, which is accompanied by overcharge voltage curves (Fig. S6 in the ESI). By contrast, a considerable average CE in SG/$ZnSO_4$ electrolyte reaches up to 99.60% over 500 cycles. The corresponding stable charge-discharge profiles with a decreasing overpotential further confirm the highly reversible cycling efficiency in the

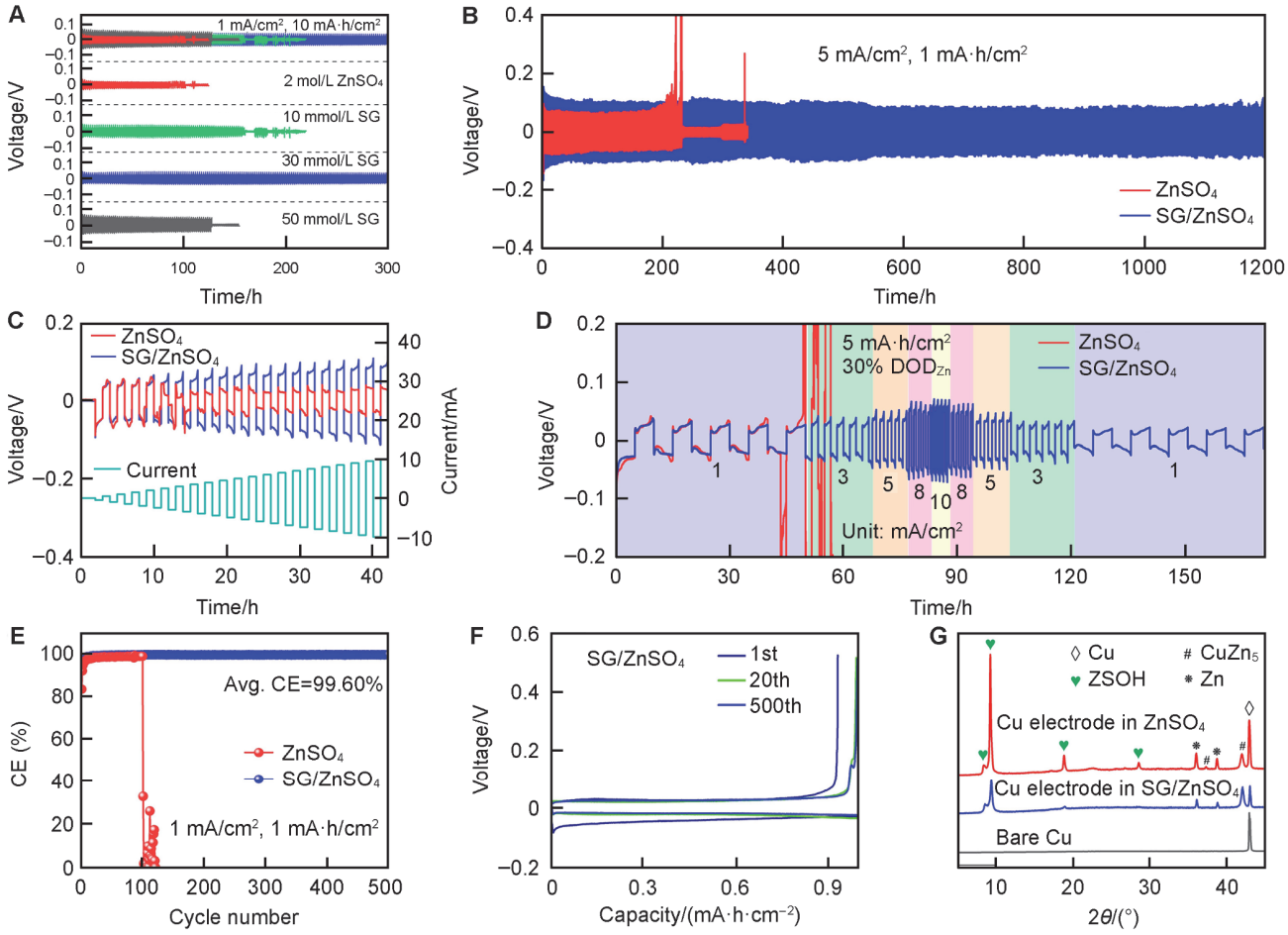

Fig. 4 Lifespan comparison of symmetric cells at 1 mA/cm², 1 mA·h/cm² with varied amounts of SG additive (A), galvanostatic cycling of Zn/Zn batteries at a current density of 5 mA/cm² in $ZnSO_4$ and SG/$ZnSO_4$ electrolytes (B), voltage profiles of symmetric cells by step increasing the current density to 10 mA/cm² (C), rate performance of Zn/Zn cells assembled using $ZnSO_4$ electrolytes with/without SG additive (D), Coulombic efficiency comparison of Zn/Cu asymmetric cells with different electrolytes (E) and corresponding voltage profiles in SG/$ZnSO_4$ electrolyte (F), and XRD patterns of plated Zn harvested from Zn/Cu cells after 25 cycles in the baseline electrolyte and designed electrolyte (G)

https://doi.org/10.1007/s40242-024-4110-9

case of SG addition (Fig. 4F). Besides, XRD tests were conducted for the Zn deposits on Cu substrates after 25 cycles under different electrolytes (Fig. 4G). Clearly, the XRD patterns in $ZnSO_4$ electrolyte display strong diffraction peaks of ZSOH byproducts, which, however, have significantly reduced intensity with the aid of SG additive. As expected, SEM images further evidence that the dendrite-free plating and suppressed parasitic reactions are achieved in SG-containing electrolyte (Fig. S7 in the ESI).

To further investigate the efficacy of SG additive, aqueous Zn-based batteries were assembled using a Zn foil anode and different cathodes, such as $V_2O_5{\cdot}1.6H_2O$ and polyaniline (PANI). Here, $V_2O_5{\cdot}1.6H_2O$ was fabricated through a conventional hydrothermal method. The corresponding crystalline phase and the nanoflake structure are identified from the XRD patterns (Fig. S8 in the ESI) and SEM images (Fig. S9 in the ESI), respectively. Fig. 5A shows two pairs of redox peaks in CV curves of $Zn/V_2O_5{\cdot}1.6H_2O$ cells under different electrolytes, corresponding to the valence change of vanadium, respectively.[43,44] With 30 mmol/L SG in $ZnSO_4$ electrolyte, the rate performance of $Zn/V_2O_5{\cdot}1.6H_2O$-based cells at diverse current densities ranging from 200 mA/g to 5000 mA/g precedes those without electrolyte additive (Fig. 5B). Evidently, the selected curves at 500 and 1000 mA/g exhibit lower polarization in the SG-containing batteries (Fig. 5C). As depicted in Fig. 5D, the battery using optimized $SG/ZnSO_4$ electrolyte presents great cycling stability of nearly 86.5% capacity retention after 1000 cycles, which is much better than that of configuration with bare $ZnSO_4$ electrolyte (48.6%). Such improved reversibility is attributed to the reduced polarization (Fig. S10 in the ESI) and suppression of dendrite growth (Fig. 5E), indicating the significant impact of SG additive in improving the performance for aqueous Zn batteries.

Furthermore, we checked the universality of SG as electrolyte additive by taking Zn/PANI cells as an example. The nanostructure of commercial PANI powders was characterized by SEM images and Raman spectra (Fig. S11 in the ESI). When coupling a Zn anode with the PANI cathode, the cell employing $SG/ZnSO_4$ electrolyte exhibits a better rate performance as compared to that with the $ZnSO_4$ electrolyte (Fig. S12 in the ESI). As expected, the cyclic durability of the Zn/PANI cell with $SG/ZnSO_4$ electrolyte was again proven at a high current density of 1000 mA/g (Fig. S13 in the ESI). These results indicate that SG is an effective electrolyte additive to stabilize aqueous batteries coupling Zn anode with diverse cathode materials.

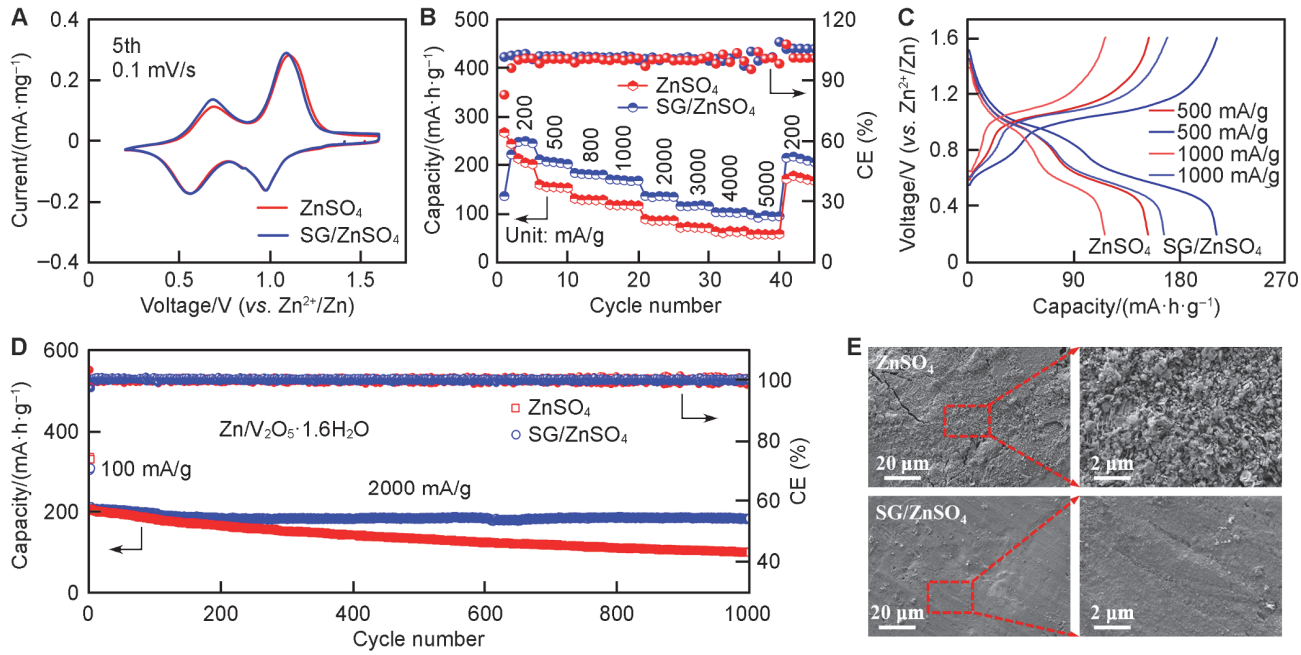

Fig. 5 Cyclic voltammetry curves of $Zn/V_2O_5{\cdot}1.6H_2O$ cells in the electrolytes with/without SG additive (A), capacities at diverse rates of different electrolytes (B) and corresponding charge/discharge voltage profiles at 500 and 1000 mA/g (C), long-term cycling behaviors of the batteries using $ZnSO_4$ and $SG/ZnSO_4$ electrolytes at 2000 mA/g (D), and SEM images of cycled Zn anodes in $Zn/V_2O_5{\cdot}1.6H_2O$ cells (E)

4 Conclusions

In summary, a green and economic electrolyte additive, SG is reported and investigated for representative aqueous $ZnSO_4$ electrolyte to improve the reversibility of Zn anodes. Mechanism analyses suggest that SG molecules are favorably absorbed on the electrode surface, which could mitigate the water-induced parasitic reactions and homogenize the Zn deposition. Remarkably, 30 mmol/L SG addition endows the Zn/Zn cells with an outstanding cyclic

https://doi.org/10.1007/s40242-024-4110-9

durability up to 1200 h at a current density of 5 mA/cm^2, significantly outperforming the benchmark $ZnSO_4$ electrolyte. Holding the merits of boosting Zn reversibility, the formulated electrolyte is applicable to improve the cycling stability of Zn batteries employing $V_2O_5{\cdot}1.6H_2O$ or PANI cathode materials. This work would promote design of efficient yet low-cost electrolyte additives for better rechargeable aqueous batteries.

Electronic Supplementary Information

Supplementary material is available in the online version of this article at http://dx.doi.org/10.1007/s40242-024-4110-9.

Acknowledgements

This work was supported by the National Natural Science Foundation of China (Nos. 21925503 and 22309167), the PhD Research Fund Project of Zhengzhou University of Light Industry, China (No. 2022BSJJZK10), the Science and Technology Project of Henan Province, China (No. 242102241045), the Natural Science Foundation of Henan Province, China (No. 242300420206) and the Specially-Appointed Professor Project of Zhengzhou University of Light Industry, China.μ

Conflicts of Interest

CHENG Fangyi is an editorial board member for Chemical Research in Chinese Universities and was not involved in the editorial review or the decision to publish this article. The authors declare no conflicts of interest.

References

[1] Zhao R., Wang H., Du H., Yang Y., Gao Z., Qie L., Huang Y., *Nat. Commun.*, **2022**, *13*, 3252.
[2] Wang L., Zhang B., Zhou W., Zhao Z., Xin Liu, Zhao R., Sun Z., Li H., Wang X., Zhang T., Jin H., Li W., Elzatahry A., Hassan Y., Fan H. J., Zhao D., Chao D., *J. Am. Chem. Soc.*, **2024**, *146*, 6199.
[3] Liu M., Yuan W., Ma G., Qiu K., Nie X., Liu Y., Shen S., Zhang N., *Angew. Chem. Int. Ed.*, **2023**, *62*, e202304444.
[4] Wang Q., Kaushik S., Xiao X., Xu Q., *Chem. Soc. Rev.*, **2023**, *52*, 6139.
[5] Li H., Zhao R., Zhou W., Wang L., Li W., Zhao D., Chao D., *JACS Au*, **2023**, *3*, 2107.
[6] Wu J., Yuan C., Li T., Yuan Z., Zhang H., Li X., *J. Am. Chem. Soc.*, **2021**, *143*, 13135.
[7] Guo X., Zhang Z., Li J., Luo N., Chai G.-L., Miller T. S., Lai F., Shearing P., Brett D. J. L., Han D., Weng Z., He G., Parkin I. P., *ACS Energy Lett.*, **2021**, *6*, 395.
[8] Wu W., Deng Y., Chen G., *Chinese Chem. Lett.*, **2023**, *34*, 108424.
[9] Di S., Nie X., Ma G., Yuan W., Wang Y., Liu Y., Shen S., Zhang N., *Energy Storage Mater.*, **2021**, *43*, 375.
[10] Liu X., Fang Y., Liang P., Xu J., Xing B., Zhu K., Liu Y., Zhang J., Yi J., *Chinese Chem. Lett.*, **2021**, *32*, 2899.
[11] Wang L., Fan G., Liu J., Zhang L., Yu M., Yan Z., Cheng F., *Chinese Chem. Lett.*, **2021**, *32*, 1095.
[12] Wang T., Tang Y., Yu M., Lu B., Zhang X., Zhou J., *Adv. Funct. Mater.*, **2023**, *33*, 2306101.
[13] Zhang L., Xiao J., Xiao X., Xin W., Geng Y., Yan Z., Zhu Z., *eScience*, **2024**, *4*, 100205.
[14] Li J., Rohrens D., Dalfollo G., Wu X., Lu Z., Gao Q., Han B., Sun R., Zhou C., Wang J., Cai Z., *Nano Mater. Sci.*, **2023**, DOI: 10.1016/j.nanoms.2023.11.004.
[15] Huang J.-Q., Guo X., Lin X., Zhu Y., Zhang B., *Research*, **2019**, *2019*, 2635310.
[16] Xiong P., Lin C., Wei Y., Kim J.-H., Jang G., Dai K., Zeng L., Huang S., Kwon S. J., Lee S.-Y., Park H. S., *ACS Energy Lett.*, **2023**, *8*, 2718.
[17] Zhao K., Fan G., Liu J., Liu F., Li J., Zhou X., Ni Y., Yu M., Zhang Y.-M., Su H., Liu Q., Cheng F., *J. Am. Chem. Soc.*, **2022**, *144*, 11129.
[18] Wang C., Hou J., Gan Y., Xie L., He Y., Hu Q., Liu S., Jun S. C., *J. Mater. Chem. A*, **2023**, *11*, 8057.
[19] Zhang W., Zhang C., Wang H., Wang H., *Chem. Res. Chinese Universities*, **2023**, *39*, 1037.
[20] Wang D., Lv D., Liu H., Zhang S., Wang C., Wang C., Yang J., Qian Y., *Angew. Chem. Int. Ed.*, **2022**, *61*, e202212839.
[21] Zheng L., Li H., Wang X., Chen Z., Hu C., Wang K., Gao G., Passerini S., Zhang H., *ACS Energy Lett.*, **2023**, *8*, 2086.
[22] Huang C., Zhao X., Hao Y., Yang Y., Qian Y., Chang G., Zhang Y., Tang Q., Hu A., Chen X., *Energy Environ. Sci.*, **2023**, *16*, 1721.
[23] Li T. C., Lin C., Luo M., Wang P., Li D.-S., Li S., Zhou J., Yang H. Y., *ACS Energy Lett.*, **2023**, *8*, 3258.
[24] Shi X., Wang J., Yang F., Liu X., Yu Y., Lu X., *Adv. Funct. Mater.*, **2023**, *33*, 2211917.
[25] Hu Z., Zhang F., Zhou A., Hu X., Yan Q., Liu Y., Arshad F., Li Z., Chen R., Wu F., Li L., *Nano-Micro Lett.*, **2023**, *15*, 171.
[26] Luo X., Zhou M., Luo Z., Shi T., Li L., Xie X., Sun Y., Cao X., Long M., Liang S., Fang G., *Energy Storage Mater.*, **2023**, *57*, 628.
[27] Hou Z., Gao Y., Zhou R., Zhang B., *Adv. Funct. Mater.*, **2022**, 32, 2107584.
[28] Kim M., Lee J., Kim Y., Park Y., Kim H., Choi J. W., *J. Am. Chem. Soc.*, **2023**, *145*, 15776.
[29] Sun P., Ma L., Zhou W., Qiu M., Wang Z., Chao D., Mai W., *Angew. Chem. Int. Ed.*, **2021**, *60*, 18247.
[30] Zhao K., Sheng J., Luo N., Ding J., Luo H., Jia X., Wang S, Fang S., *J. Colloid Interf. Sci.*, **2024**, *664*, 816.
[31] Wang J., Qiu H., Zhao Z., Zhang Y., Zhao J., Ma Y., Li J., Xing M., Li G., Cui G., *Chem. Res. Chinese Universities*, **2021**, *37*, 328.
[32] Wan J., Wang R., Liu Z., Zhang L., Liang F., Zhou T., Zhang S., Zhang L., Lu Q., Zhang C., Guo Z., *ACS Nano*, **2023**, *17*, 1610.
[33] Xin T., Zhou R., Xu Q., Yuan X., Zheng Z., Li Y., Zhang Q., Liu J., *Chem. Eng. J.*, **2023**, *452*, 139572.
[34] Wang N., Chen X., Wan H., Zhang B., Guan K., Yao J., Ji J., Li J., Gan Y., Lv L., Tao L., Ma G., Wang H., Zhang J., Wang H., *Adv. Funct. Mater.*, **2023**, *33*, 2300795.
[35] Zhong Y., Cheng Z., Zhang H., Li J., Liu D., Liao Y., Meng J., Shen Y., Huang Y., *Nano Energy*, **2022**, *98*, 107220.
[36] Yan M., Xu C., Sun Y., Pan H., Li H., *Nano Energy*, **2021**, *82*, 105739.
[37] Zhao K., Liu F., Fan G., Liu J., Yu M., Yan Z., Zhang N., Cheng F., *ACS Appl. Mater. Interfaces*, **2021**, *13*, 47650.
[38] Zhao Z., Zhao J., Hu Z., Li J., Li J., Zhang Y., Wang C., Cui G., *Energy Environ. Sci.*, **2019**, *12*, 1938.
[39] Chen Y., Ma D., Ouyang K., Yang M., Shen S., Wang Y., Mi H., Sun L., He G., Zhang P., *Nano-Micro Lett.*, **2022**, *14*, 154.
[40] Jin Y., Han K. S., Shao Y., Sushko M. L., Xiao J., Pan H., Liu J., *Adv. Funct. Mater.*, **2020**, *30*, 2003932.
[41] Yin J., Liu H., Li P., Feng X., Wang M., Huang C., Li M., Su Y., Xiao B., Cheng Y., Xu X., *Energy Storage Mater.*, **2023**, *59*, 102800.
[42] Qin R., Wang Y., Zhang M., Wang Y., Ding S., Song A., Yi H., Yang L., Song Y., Cui Y., Liu J., Wang Z., Li S., Zhao Q., Pan F., *Nano Energy*, **2021**, *80*, 105478.
[43] Sun C., Wu C., Gu X., Wang C., Wang Q., *Nano-Micro Lett.*, **2021**, *3*, 89.
[44] Cao Z., Zhu X., Xu D., Dong P., Chee M. O. L., Li X., Zhu K., Ye M., Shen J., *Energy Storage Mater.*, **2021**, *36*, 132.